Single bubble deformation and breakup in simple shear flow

Exp Fluids (2008) 45:917–926
DOI 10.1007/s00348-008-0509-1

RESEARCH ARTICLE

Single bubble deformation and breakup in simple shear flow

Nadina Müller-Fischer · Philip Tobler · Marco Dressler · Peter Fischer · Erich J. Windhab

Received: 14 March 2008 / Revised: 12 April 2008 / Accepted: 14 April 2008 / Published online: 1 May 2008

Abstract Experiments in a parallel band apparatus and a transparent concentric cylinder device allow the observation of bubble deformation (shape and orientation) and breakup as a function of the viscosity ratio λ and the Capillary number Ca. For viscosity ratios between 3.1×10^{-7} and 6.7×10^{-8}, critical Capillary numbers Ca_c for bubble breakup between 29 and 45 are found. It is furthermore shown that in the given parameter space no clear distinction between tip breakup and fracture can be made for bubbles.

List of symbols

B	minor axis (m)
Ca	Capillary number
Ca_c	critical Capillary number
D	deformation
g	gravity constant (m s^{-2})
$\dot{\gamma}$	shear rate (s^{-1})
η_{disp}	disperse phase viscosity (Pa s)
η_{cont}	continuous phase viscosity (Pa s)
L	major axis (m)
λ	viscosity ratio
r	radius (m)
$r_{B,\ orbit}$	radius of bubble orbit (m)
R_i	radius of inner cylinder (m)
R_o	radius of outer cylinder (m)
Re	Reynolds number
ρ	density (kg m^{-3})
σ	interfacial tension (N m^{-1})
Θ	rotation angle (°)
v_{St}	Stokes velocity (m s^{-1})
ω	angular velocity (s^{-1})
x_B	bubble diameter (m)

N. Müller-Fischer · P. Tobler · M. Dressler · P. Fischer · E. J. Windhab
Institute of Food Science and Nutrition, ETH Zurich, 8092 Zurich, Switzerland

P. Fischer
e-mail: peter.fischer@ilw.agrl.ethz.ch

N. Müller-Fischer (✉)
Bühler AG, 9240 Uzwil, Switzerland
e-mail: nadina.mueller-fischer@buhlergroup.com

1 Introduction

The deformation and breakup of bubbles in a surrounding fluid is an important unit operation in foaming processes. To design foaming processes that allow tailor-made foams to be produced there is considerable interest to study the mechanics of bubble breakup and flow (Müller-Fischer et al. 2007a, b). In foaming processes bubbles are subjected to flow stresses such as viscous friction (shear and elongation) or inertia stresses (turbulent flow). Depending on the strength of applied stresses, deformation and eventually break up into smaller bubbles occurs. In most cases, research focuses on bubble breakup in turbulent flow and on bubble break-up for Re → ∞. Excellent overviews to the area are available (e.g. Lasheras et al. 2002; Risso and Fabre 1998; Revuelta et al. 2006; Rodríguez-Rodríguez et al. 2006; Gordillo and Perez-Saborid 2006). On the other hand, research on single bubble mechanics is rare. Studies by Canedo et al. (1993) and Rust and Manga (2002) were focused on bubble deformation, whereas reports on single bubble breakup in simple shearing flow have not been reported. In particular, no data on critical deformations exist for the boundary conditions applied in this work, i.e.

laminar flow and low Re-numbers. In contrast to this, the correlation of deformation and breakup of single droplets to the external flow conditions has been widely studied (e.g. Acrivos 1983; Grace 1982; Rallison 1984; Stone 1994). A considerable drawback of this situation is that models for single bubble mechanics do not exist and, thus, models for droplet mechanics are used instead to describe bubble mechanics. As we will show later, this approach is justified for bubble deformation but fails in case of bubble breakup based on our investigation. In the following we therefore will briefly review droplet deformation models assuming that certain cross correlation can be made.

A spherical aggregate with deformable interface such as a droplet or bubble placed in steady simple shear flow at low Reynolds number deforms with a time-dependent shape and orients until it reaches a steady deformation or breaks up into smaller aggregates. The steady state shape and orientation depends on (1) the ratio of the viscosity λ of the dispersed media relative to the surrounding fluid, (2) the Capillary number Ca, and (3), if present, the concentration of surfactant determining the interfacial tension. Ca is the ratio of shear stresses generated in the flow that deform the droplet or bubble and interfacial tension-related stresses represented by the Laplace pressure that tend to keep the spherical shape. The force balance of stresses generated in a flow field that deform a droplet and interfacial tension stresses that resist the deformation is given by

$$Ca = \frac{\eta_{\text{cont}} \dot{\gamma} x_{\text{B}}}{2\sigma}. \tag{1}$$

Here η_{cont} is the viscosity of the continuous phase, $\dot{\gamma}$ the shear rate, x_{B} the droplet diameter, and σ the surface tension.

At low deformations, the deformed droplet has an ellipsoidal shape. In a two-dimensional approach assuming an axisymmetric droplet shape, its major axis L and its minor axis B as well as the rotation angle versus the principal axis of flow θ define the droplet shape in flow. Figure 1 shows a schematic drawing of an initial, spherical droplet and a deformed, ellipsoidal droplet. The deformation parameter D first introduced by Taylor (1934) can be used to characterize the degree of deformation for modest shape changes:

$$D = \frac{L - B}{L + B}. \tag{2}$$

D is 0 for a sphere and asymptotically approaches unity for higher deformed, long and slender bodies. The experimental results by Canedo et al. (1993) justify the utilization of the droplet deformation models for description of bubble deformation. For small deformations, $D \leq 0.3$, the steady-state geometry of a bubble can be described using Taylor theory that originally was derived for droplet deformation (Taylor 1934):

$$D = Ca \frac{19\lambda + 16}{16\lambda + 16}, \tag{3}$$

where λ is the ratio of the disperse phase viscosity to the continuous phase viscosity. For $Ca \ll 1$ and $\lambda \ll 1$, the droplet is nearly spherical

$$Ca \cong D. \tag{4}$$

For highly deformed aggregates, where the shape deviates strongly from an ideal ellipsoid, the dimensionless length L/x_{B}, obtained by dividing the longer axis of the deformed body L by the original radius x_{B} is an appropriate measure of deformation (Bentley and Leal 1986). At deformations, $L \gg x_{\text{B}}$, droplets or bubbles are elongated with pointed ends. Using slender body theory and assuming droplets to be circular in cross section, Hinch and Acrivos (1980) predict for $Ca \gg 1$, $\lambda \ll 1$ and Re $\ll 1$:

$$\frac{L}{x_{\text{B}}} \cong 3.45 Ca^{0.5}. \tag{5}$$

Associated with the deformation of a deformable aggregate under shear, there is an orientation process which makes the deformed droplet or bubble reach an angle θ with respect to the flow direction. This angle is by definition 45° at rest and decreases with increasing applied shear-rate as the aggregate becomes aligned with the flow direction more and more. This flow-induced orientation depends on the Capillary number and was first expressed as a linear relationship (see Cerf 1951; Chaffey and Brenner 1967). From experimental observation, it has however become clear that θ does not depend linearly on Ca when the shear-rate increases. Hence, a non-linear description must be used. Cox (1969) published his theoretical analysis for orientation under shear flow which follows as:

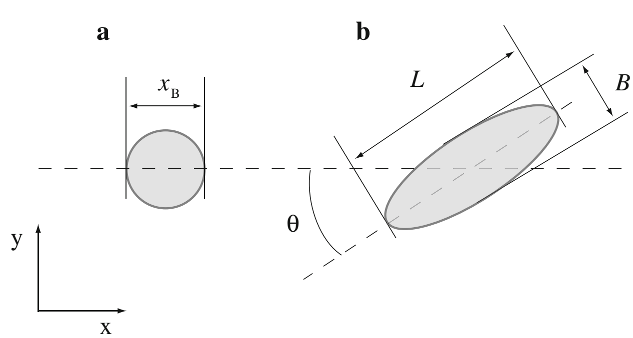

Fig. 1 Parameters describing droplet and bubble deformation: x_{B} droplet or bubble diameter, L major axis, B minor axis, θ rotation angle. **a** Initial, undeformed droplet or bubble shape and **b** deformed droplet or bubble

$$\theta = \frac{\pi}{4} - \frac{1}{2}\arctan\left(\frac{19\lambda Ca}{20}\right). \quad (6)$$

In this case, the viscosity ratio between suspended media and continuous phase is taken into account. Hinch and Acrivos (1980) proposed a model for high Capillary numbers in systems in which the disperse phase has low viscosity compared to that of the suspending liquid:

$$\theta = \arctan\left(0.359 Ca^{-0.75}\right). \quad (7)$$

The phenomenological model of Maffetone and Minale (1999) assumes ellipsoidal aggregate form and describes the orientation as:

$$\theta = \frac{1}{2}\arctan\left(\frac{f_1}{Ca}\right), \quad (8)$$

where f_1 is given by:

$$f_1 = \frac{40(\lambda + 1)}{(2\lambda + 3)(19\lambda + 16)}. \quad (9)$$

Experimental work on droplets using Eqs. 6 and 7 showed good agreement between theory and experiments for relatively large deformations (Canedo et al. 1993; Rust and Manga 2002). However, the Cox equation (Eq. 6) fails to predict experimental trends of θ for $\lambda \leq 1$. The most appropriate range of applicability of the Cox theory is for $\lambda \gg 1$, where good agreement has been found with experimental data. All above mentioned theories for droplet mechanics (Eqs. 2–10) have been widely explored both experimentally (Cox 1969; Taylor 1934; Bentley and Leal 1986; Grace 1982; Guido and Greco 2001; Guido and Villone 1998; Guido et al. 1999; Torza et al. 1972) and in numerical calculations (Pozrikidis 1993; Rallison 1981). For reviews on droplet mechanics see also the overview articles by Stone (1994) or Fischer and Erni (2007) and references therein.

The only fairly recent investigations of bubble behavior under simple shear were published by Canedo et al. (1993) and Rust and Manga (2002). Rust and Manga reached bubble deformations D of 0.94 corresponding to $L/x_B = 32$ but did not reach bubble breakup neither during shearing nor during relaxation. Their experiments comprised shape data for bubbles for $0.02 < Ca < 7.1$ reaching both spheroidal and slender body model regimes described by Eqs. 4 and 5, respectively, as well as the transition between small and large deformation limits. Their data agreed well with Eq. 4 for values of $\lambda \to 0$ and Re $\ll 1$ up to $Ca \leq 0.5$ and with Eq. 5 for $Ca > 1$ and values of $\lambda \ll 1$ and Re $\ll 1$. Canedo et al. (1993) measured experimentally the deformation of air bubbles suspended in polybutene oil in a concentric cylinder device applying simple shear flow conditions. They found that bubble cross-sections are elliptical and suggested that deformations as a function of Ca are slightly less than predicted by Eq. 5. Their data for $3 < Ca < 50$ were well described by

$$\frac{L}{x_B} = 3.1 Ca^{0.43}. \quad (10)$$

As in bubble deformation, we can describe bubble breakup in laminar flow at low Reynolds numbers by drawing similarities to droplet breakup. A droplet is unable to maintain a steady shape as soon as flow-induced stresses exceed the interfacial tension stress. Consequently, the droplet undergoes a transient, continuous stretching which eventually results in droplet breakup. The critical Capillary number Ca_c is defined as the point where no stable droplet or bubble shape exists because a critical stress exceeds the stabilizing interfacial tension σ and leads to breakup. The critical Capillary number depends on the type of flow (simple shear flow, mixed shear-elongational flow, pure extensional flow) and the viscosity ratio λ of disperse to continuous phase. Ca is, thus, commonly plotted as a function of λ. Depending on the chosen parameters, generation of equally sized daughter drops with and without satellite droplets, tip streaming, and droplet rupture may occur (e.g. Stone et al. 1986). The experimental results on droplet breakup were summarized by Grace (1982) for viscosity ratios between $10^{-6} \leq \lambda \leq 10^3$.

Droplet mechanics in the low viscosity ratio regime that is typical for bubbles requires high Capillary numbers to burst and to attain steady slender shapes at very large, under-critical deformations. The lower the viscosity ratio, the greater the sustainable deformation and consequently the higher the critical Capillary number. For such deformations, droplets and bubbles deviate from ellipsoidal shape considerably and develop pointed ends. Tip streaming in simple shear flows is a mode of droplet breakup in which the droplet develops a sigmoidal shape and a stream of tiny droplets is ruptured off the pointed ends/tips of the drop. Tip streaming is observed at under-critical Capillary number for drops (Grace 1982; Taylor 1934). De Brujin (1993) found that tip streaming only occurs if the viscosity ratio is smaller than unity and if interfacial tension gradients can develop, i.e. in the presence of surfactants or impurities in the fluid.

2 Materials and methods

2.1 Materials

The basic modeling assumptions that should be closely followed in experimental studies are: steady creeping flow with negligible inertia effects, incompressible Newtonian fluids, no buoyancy effects (i.e. no body forces), no wall effects (i.e. unbounded suspending flow-field), and no heat or mass transfer (isothermal conditions). For bubbles, the boundary conditions of incompressibility and no buoyancy can not be fulfilled. Due to the large density difference between air bubble and continuous fluid phase, we therefore selected only highly-viscous materials as the continuous fluid phase. Consequently, the corresponding low viscosity ratios λ between 10^{-6} and 10^{-7} determines the rising velocity of bubbles to be sufficiently slow for steady state experiments. The rising velocity or Stokes velocity is computed as:

$$v_{\mathrm{St}} = \frac{1}{18} \times \frac{g \Delta\rho x_{\mathrm{B}}^2}{\eta_{\mathrm{cont}}}, \tag{11}$$

where g denotes the gravity acceleration and $\Delta\rho$ the density difference between gas bubble and surrounding continuous phase.

Glucose syrups of different viscosities (C*BioSweet 11160, BC*Sweet 01175, C*BioSweet 11144, Blattmann Cerestar, Switzerland) and silicone oils (AK 60000, AK 100000, AK 300000, Wacker-Chemie, Germany) were used as continuous phase. Table 1 shows the viscosity, density, surface tension, and rising velocity resulting for a bubble of diameter 2 mm in glucose syrups and silicone oils, respectively. The disperse phase was air and no emulsifier was added to the continuous phase.

The Newtonian flow behavior of glucose syrups and silicone oils as well as temperature dependent viscosities were obtained by a rotational rheometer (Anton Paar Physica MCR 300, Austria). Surface tension measurements were carried out at 18°C using the drop detachment method for the glucose syrups. The density of the glucose syrup needed for the surface tension measurements was determined with a density meter using the oscillating U-tube method (Anton Paar DMA-38, Austria). The values for the surface tension and density for silicone oils are provided by the manufacturer.

2.2 Parallel band apparatus

To investigate deformations and bubble break-up in simple shear, two experimental devices were used: the parallel band apparatus and a transparent Couette flow cell. The parallel band apparatus (see Fig. 2) consists of two metal bands that run around several rolls inside a container of 30 cm in length, 18 cm in width and 6 cm in depth. Metallic bands of 3.3 cm width were used, tightened with springs to avoid bending effects. The motion of the ribbons was controlled independently by two motors using a computer-control scheme based on direct image analysis of the bubble and PID-controlled motor adjustment (Birkhofer et al. 2005) which continuously adapts the flow parameters in order to keep the observed bubble at the requested position for indefinite times. Steady-state deformation of sheared bubbles can be observed accurately. The bubble behavior was recorded with a CCD camera (Sony DFW-V500, Japan) placed in azimuthal position ($x-y$ plane of bubble as depicted in Fig. 1). The diameter of the undeformed bubble and the major and minor axes of the sheared bubble were determined by evaluating the images using *image J* (Version 1.35n, National Institutes of Health, USA). The pixel-millimeter conversion factor was determined via the known band distance. Temperature of 18°C was controlled via the double-walled base plate of the container cooled via a water-circulating bath. The shear-rate of 1.8–17.4 s^{-1} is set as the ratio between the relative speed of the bands and the gap between them, which is set to 9.76 mm for all experiments. The velocity gradient developed in the parallel band apparatus is linear and laminar. Air bubbles were placed between the two bands using a syringe. The radius of $x_{\mathrm{B}} \leq 2.75$ mm of the undeformed bubbles is chosen in order to avoid edge effects, i.e. bound flow conditions. A schematic drawing of the shear cell, computer control mechanism, and the entire setup can be found elsewhere (Birkhofer et al. 2005).

2.3 Transparent concentric cylinder device

A transparent concentric cylinder device is used (see Fig. 3) to extend the shear rate regime of the parallel band apparatus and to achieve in combination with highly-viscous silicone oil bubble breakup. In the present version of the device only the inner cylinder rotates and as a result, the bubbles revolve around the cylinder axis. The advantages of the transparent concentric cylinder device compared to the

Table 1 Viscosity, density, surface tension, and rising velocity for Re < 0.25 (Eq. 11) of air bubbles

Continuous phase	Viscosity (Pa s)	Density (kg m^{-3})	Surface tension (mN m^{-1})	Rising velocity (mm s^{-1})
Glucose syrup 11160	28.6	1,409	80.74	0.11
Glucose syrup 01175	97.3	1,412	80.64	0.03
Glucose syrup 11144	141.4	1,423	80.69	0.02
AK 60000	58.2	970	21.5	0.04
AK 100000	97	970	21.5	0.02
AK 300000	290	970	21.5	0.007

Values are reported for 18°C (glucose syrups) and 25°C (silicone oils), and bubble diameter of 2 mm

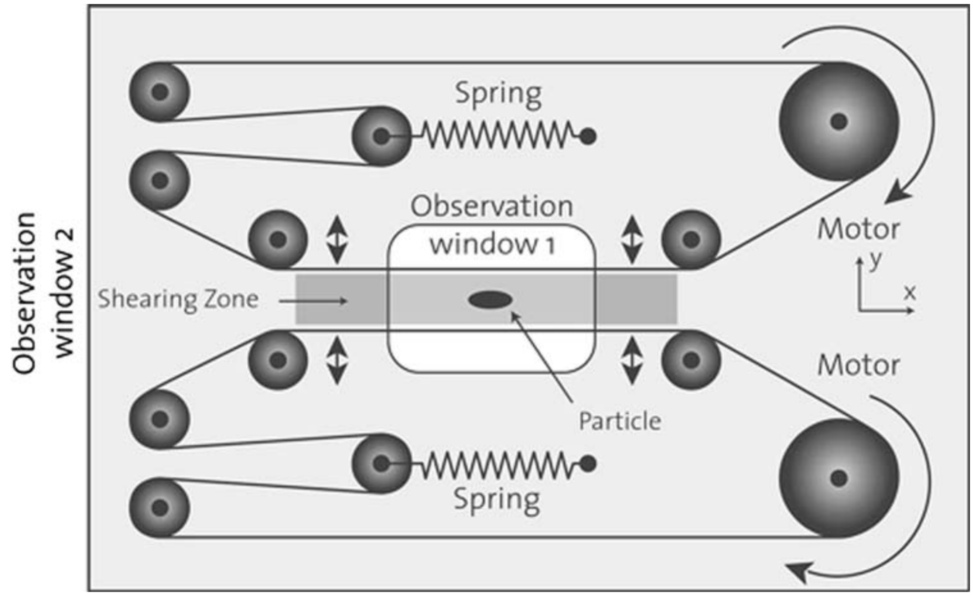

Fig. 2 Diagram of the shear cell (*top view*) (Birkhofer et al. 2005)

band apparatus are, in particular, higher achievable Capillary numbers even though gap width is larger and fixed (higher shear rate, four times lower surface tension of silicone oil).

The device was composed of an inner cylinder made of Polyvinylchlorid (PVC) with diameter 117.5 mm and height 250.0 mm, an outer cylinder made of plexiglass with inner diameter 141.0 mm and height 300.0 mm, an injection port with a silicone-sealing allowing the introduction of air bubbles into the gap, two CCD cameras (DFW-V500, Sony), and illumination setup. The shear rate $\dot{\gamma} = 1.8 - 52.1\ \mathrm{s}^{-1}$ was computed according to DIN (1976) as:

$$\dot{\gamma}(\mathrm{r}) = \frac{1}{r^2_{\mathrm{B,\,orbit}}} \times \frac{2R_i^2 R_o^2}{(R_o^2 - R_i^2)} \times \omega. \tag{12}$$

To place a bubble into the gap, a syringe is inserted into the gap through the injection port at the bottom of the gap. One CCD-camera looks sidewards onto the plexiglass-cylinder and captures movies of bubble size and break-up. The second camera is placed below the transparent concentric cylinder to assess the position of the bubble in the gap. Pictures of the undeformed bubble plus a ruler are taken to determine the bubble size using *image J*. The rotational speed of the inner cylinder is step-wise increased with long waiting periods until break-up occurs.

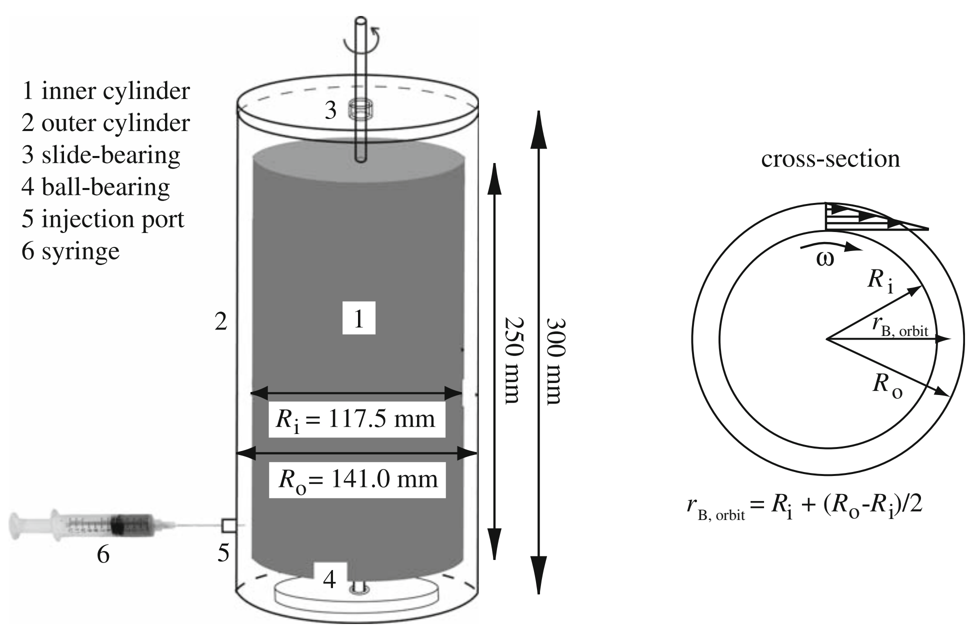

Fig. 3 Illustration of the transparent concentric cylinder device: *side view* and *cross-section*

3 Results and discussion

3.1 Bubble deformation in parallel band apparatus

Figure 4 shows the typical development of bubble deformation in simple shear in the parallel band apparatus. As soon as shearing is started, the spherical bubble undergoes a transient shear deformation. The bubble changes from spherical via ellipsoidal to sigmoidal with pointed ends (frames 1–5). At the same time, the major bubble axis aligns more and more with the flow direction ($0° < \theta < 45°$). Maximum deformation and alignment represent the steady shear state (frame 5). Upon stopping the shear bands, bubbles relaxed from the sigmoidal shape back to ellipsoids and spheres again (frames 6–9). During relaxation, the bubble angle again approaches 45°. The relaxation process is approximately inverse to the deformation process.

Steady-state maximum deformation and alignment at different Capillary numbers in simple shear flow are summarized in Fig. 5. With increasing Capillary number the deformation increases while the orientation angle approaches 0° for very high shear stresses. In this case, the sigmoidal form as well as the pointed ends of the bubbles become more and more pronounced.

The determined steady deformations D of the bubbles as a function of Ca are plotted in Fig. 6a. Here data from experiments with bubbles of different diameter (0.86 mm $\leq x_B \leq$ 2.75 mm) subjected to shear rates between 3.5 and 17.4 s^{-1} obtained with glucose syrups of viscosities from 28.6 to 141.4 Pa s and resulting in viscosity ratios between 6.4 and 1.3 × 10^{-7} are combined to examine relationships between bubble geometry and Capillary number. The deformation parameter D scales proportionally to Ca for $Ca < 1$ and then asymptotically approaches a value of 0.89 for increasing Capillary number. These results are compared to data from literature and to models. In Fig. 6a the deformation parameter D measured by Rust and Manga

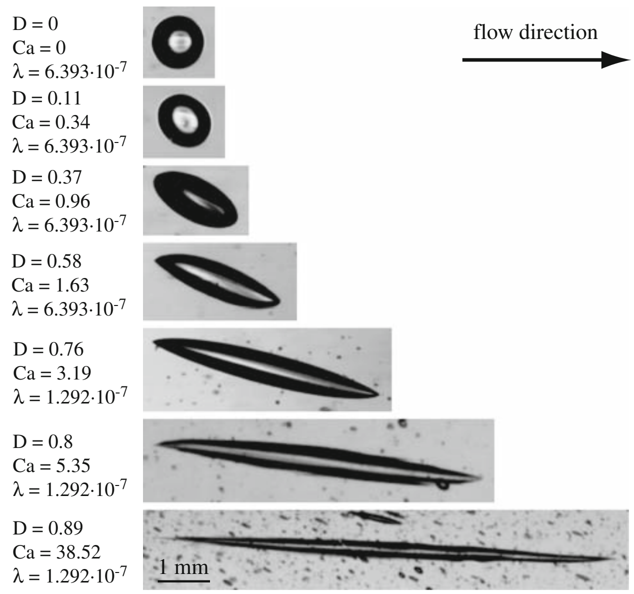

Fig. 5 Maximum steady-state bubble deformation $D = (L-B)/(L+B)$ and orientation at different Capillary numbers

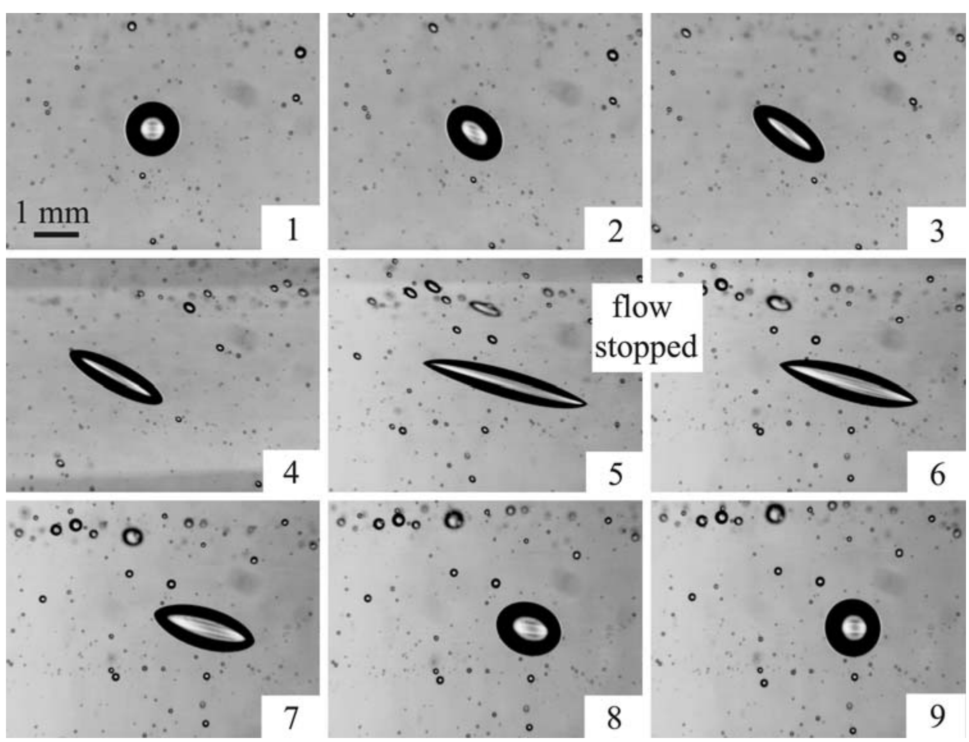

Fig. 4 Air bubble deformation (frames 1–5) and relaxation (frames 5–9) in simple shear flow as a function of elapsed time (parallel band apparatus, glucose syrup C*BioSweet 11160, $\lambda = 6.0 \times 10^{-7}$, $\dot{\gamma} = 10.5$ s^{-1}, scale in frame 1)

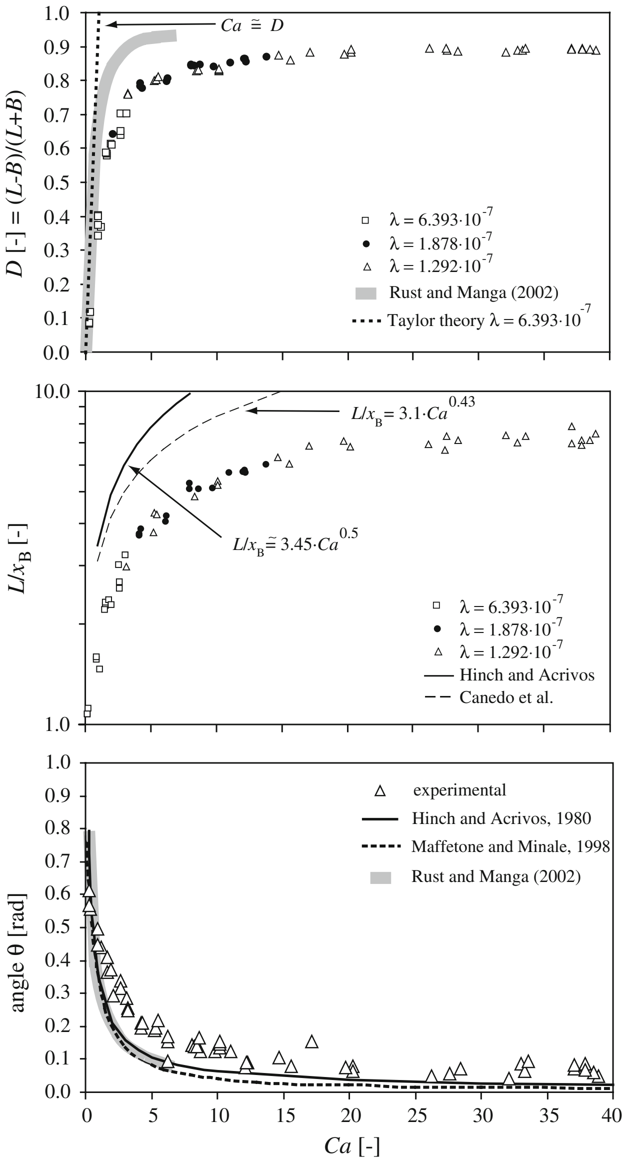

Fig. 6 **a** Deformation parameter D as a function of the Capillary number Ca for bubbles in simple shear flow. Own experimental results, compared to results obtained by Rust and Manga (2002, *thick grey line*) and fit to Taylor theory (*dotted line*). **b** Deformation parameter L/x_B as a function of the Capillary number Ca for bubbles in simple shear. *Symbols* represent measured values, the *solid line* represents the model prediction by Hinch and Acrivos (1980), the *dashed line* the model for Canedo et al. (1993). **c** Steady orientation of bubbles in simple shear flow as a function of the Capillary number Ca. The *line* is the theoretical relationship by Hinch and Acrivos (1980, Eq. 7), the *dashed line* the model by Maffetone and Minale (1999, Eq. 8), the *thick gray line* corresponds to results obtained by Rust and Manga (2002) and the *symbols* represent our experimentally obtained values

(2002) (data up to Ca = 10) is shown as well as the prediction of the Taylor model. Rust and Manga (2002) investigated bubble deformation at very low viscosity ratios of $\lambda = O(10^{-7})$ up to Ca = 7.1. No breakup was achieved. In own experiments shown in Fig. 6a, a five-times higher Capillary number of 38.9 was achieved but still no bubble breakup occurred. Higher Capillary number could not be achieved due to (1) limitation in upper shear rate above which wake formation occurs and (2) limitation in the control software, i.e. difficulty to keep bubbles in place via camera-/computer-controlled adaptation in shear rate for relative band velocities above 0.17 m s^{-1}. Qualitatively, the $D = \mathrm{f}(Ca)$ functions are similar to results by Rust and Manga (2002), but absolute values show differences. In contrast to Rust and Manga's findings, the slope of our curve is lower at low Capillary numbers and the curve deviates from Taylor theory ($Ca \cong D$) already for very low Ca number. In addition, Rust and Manga reached bubble deformations up to values of 0.94 at Capillary number of 7.1, whereas we obtained a maximum D-value of 0.89 at Capillary numbers from approximately 25 to 38.9 (Fig. 6a).

Figure 6b shows the deformation parameter parameter L/x_B valid for high deformations as a function of the Capillary number. Both models by Hinch and Acrivos (1980, Eq. 5) and Canedo et al. (1993, Eq. 10) show similar trends but overestimate the measured data. On the other hand, the assumption of Hinch and Acrivos that the bubble cross-section is circular is most probably not fulfilled at large bubble deformations. Canedo et al. (1993) demonstrated the cross-section to be ellipsoidal. They found similar deviations of model predictions by Hinch and Acrivos from their experiments on bubble deformation in simple shear obtained in a concentric cylinder shear gap. In our experiments with the parallel band apparatus, the cross-section was not observed.

Figure 6c shows the orientation angle θ as a function of the Capillary number Ca. The experimental results are compared to the slender body theory by Hinch and Acrivos (1980, Eq. 7), the phenomenological non-equilibrium thermodynamical model of Maffetone and Minale (1999, Eq. 8) and data measured by Rust and Manga (2002). The trends of the curve progression of experimental data and of the two models are again similar. Bubble orientation received from experiments in the parallel band apparatus shows less alignment into the flow direction. This tendency was expected for the comparison of experimental data to the model by Maffetone and Minale model since it assumes the droplets to be of ellipsoidal, prolate form while oblate bubbles are excluded from this model.

The deviation of the obtained results from data presented by Rust and Manga (Fig. 6) needs attention. In particular, the deviation for the deformation parameters D and L/x_B suggests some systematic error in either our work or the work of others. Possible reasons for systematic errors are higher curvature effects due to confinement and bound flow conditions (which over predicts deformation), limitation in image analysis (which under estimates the deformation), the influence of surfactants (which leads to higher deformation), and limited validity of the used models. Since literature data are also not consistent and since we are not in the position to evaluate the role of surfactants and impurities in previous work, we will only discuss sources of errors for our results: (1) The optical resolution of the used CCD camera is limited and, as a consequence, thin and pointed ends of the deformed bubbles might not be captured entirely, (2) the optical contrast between bubble and continuous phase is not very strong (see Fig. 5). Both effects lead to an incorrect determination of the major axis, inaccurate fitting to an ellipsoid, and to wrong estimation of the deformation parameters D and L/x_B. We consider a systematic error of about 10% which would lead to comparable results to findings by Rust and Manga (2002) and Canedo et al. (1993). In future experiments, it is suggested to use high speed cameras equipped with appropriate magnification lenses as well as improved illumination. The influence of surfactants or impurities was tested for all used materials in long term interfacial tension measurements (detachment experiments) and was considered to be negligible. Deviations between experimental data and model prediction for L/x_B may additionally be increased due to the unsolved issue of oblate or prolate shape of the deformed bubble (see Canedo et al. 1993; Maffetone and Minale 1999). This subject should be addressed in future experimental and modeling efforts.

3.2 Bubble breakup in transparent concentric cylinder device

Bubble breakup was observed in the transparent concentric cylinder device with three different viscous silicone oils used as continuous phase. Since the camera was fixed in place and the bubble revolved around the cylinder axis, the bubble changed its location from one picture to the next, moving from right to left. Figures 7 and 8 show pictures of the entire bubble and of the bubble tip during breakup, respectively. The deformed bubble (Fig. 7, frame 1) is close to an ellipsoidal shape with thin pointed ends. Its axis nearly aligns with the flow direction. The second picture (frame 2) shows pronounced beginning of tip breakup and points out the limitations in image capturing: it gives the impression of an open bubble tip. Additionally, an earlier broken-off small bubble can be seen on the right hand side of frame 2. In frame 3, the actual tip break-off is shown: a small, ellipsoidal daughter bubble has separated from the mother bubble.

Figure 8 focuses on the tip and the contour of the bubble during birth of a daughter bubble. The major axis of the deformed bubble orients into the flow direction of the sheared continuous phase (frame 1). A thin filament is torn off (frame 2) which partially relaxes to an ellipsoid after breakup (frame 3). The observed type of breakup is obviously a tip breakup, not total fracture. Fracture would separate the bubble into two or three almost equally sized bubbles with a few tiny satellite drops in between. These two breakup mechanisms are clearly distinguishable for droplets (e.g. de Bruijn 1993; Grace 1982) but no clear distinction between tip breakup and fracture could be experimentally found for bubbles. Instead a gradual increase in size of the daughter bubbles was found.

De Bruijn (1993) closely investigated potential reasons for tip breakup in the case of emulsions, namely the viscosity ratio and the presence of surfactants. He found that tip breakup only occurs for viscosity ratios much smaller than unity and if interfacial tension gradients could develop, resulting in reduced interfacial tension at the tips. Tip breakup did not occur at extremely low surfactant concentration, nor at high levels where drop coverage by surfactant was guaranteed. In our case, the condition $\lambda \ll 1$ is fulfilled, but there is no added surfactant which would cause an interfacial tension gradient. From our findings, we conclude that tip breakup occurs preferentially for bubbles even if there is no surface tension gradient.

Identical to the findings in the parallel band apparatus, bubble breakup was never observed during bubble

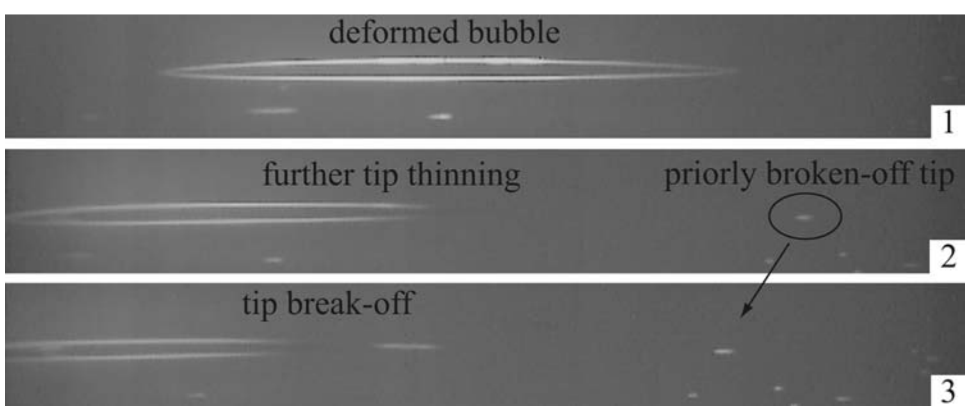

Fig. 7 Air bubble before and during tip breakup in simple shear obtained in the transparent concentric cylinder device (air bubble in silicone oil AK 100000, viscosity ratio $\lambda = 1.96 \times 10^{-7}$, $Ca_c = 33.7$)

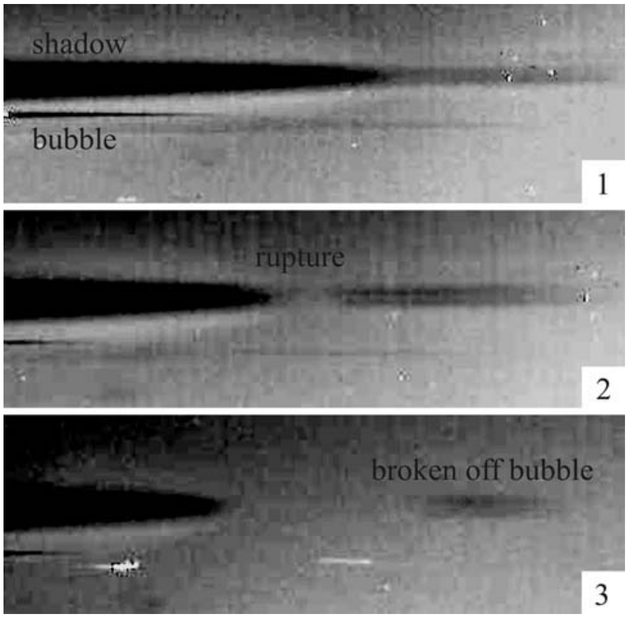

Fig. 8 Tip breakup in simple shear obtained in the transparent concentric cylinder device. In each picture, the *upper object* is the shadow of the bubble, the *lower* one the bubble itself. Breakup can be observed more easily by looking at the *shadow* due to its 2-D projection nature (air bubble in silicone oil AK 60000, viscosity ratio $\lambda = 3.09 \times 10^{-7}$, $Ca_c = 32$)

relaxation in the transparent concentric cylinder device, either for subcritical or critical Capillary numbers. Upon stopping the flow, bubbles slowly relaxed to their original spherical shapes. Rayleigh instabilities were not observed either. Contrary to what is commonly observed for droplets (Stone et al. 1986), no bubble breakup was observed during bubble relaxation.

Figure 9 shows the experimentally found relation between viscosity ratio λ and critical Capillary number Ca_c for both air bubble and droplet breakup. Bubble breakup was reached for different viscosity ratios between 3.09×10^{-7} and 6.67×10^{-8}, corresponding to critical Capillary numbers between 29.1 and 44.7. The critical *Ca*-number was found to be higher at lower viscosity ratios, as expected from published results (Grace 1982) on droplets. Comparison of the results with literature data can only be made with publications dealing with droplets, since, to the best of our knowledge, no results on bubble breakup in this parameter space (Re $<$ 0.5, laminar flow) have ever been published. Data by Grace (1982) in a similar viscosity ratio domain (down to 10^{-6}) were achieved using low viscosity drops in a high viscosity surrounding fluid. These data are depicted in Fig. 9, in addition to the obtained data for bubble breakup. The critical Capillary numbers found for bubble breakup are lower than an extrapolation of Grace's for droplet fracture would indicate, but higher than an extrapolation of Grace's for droplet tip breakup. Results for

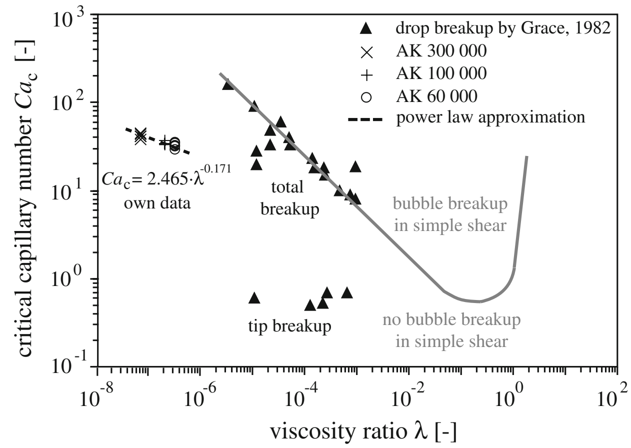

Fig. 9 Bubble breakup in simple shear obtained in the transparent concentric cylinder device. Data for air bubbles are compared to data from Grace for droplets (Grace 1982) (*lines* are to guide the eye)

bubble breakup achieved in the transparent concentric cylinder device (Fig. 9) indicate that the highest Capillary number of 38.9 achieved in parallel band apparatus experiments (see Fig. 6a) were just in the critical domain for breakup. Extrapolation of the data shown in Fig. 9 suggests that breakup should have occurred at $Ca_c = 37.8$. Naturally, such an extrapolation can only provide an approximate value.

4 Conclusion

Experiments in a parallel band apparatus and a transparent concentric cylinder allowed the observation of bubble deformation and breakup, respectively. It was shown in parallel band experiments that bubbles can be deformed strongly without achieving breakup, that breakup does not happen during relaxation and that the deformed bubbles have very thin, pointed ends. Bubble breakup in experiments using the transparent concentric cylinder were achieved at Capillary numbers *Ca* in the range of 29–45. The corresponding viscosity ratios were between 3.1×10^{-7} and 6.7×10^{-8}. Such high critical Capillary numbers explain why very small bubbles can only be achieved at high shear rates during dispersing, i.e. foaming. Grace found two different breakup mechanisms for low viscous droplets: total fracture and tip streaming. Bubble breakup was found to be different from drop breakup in two distinct ways: (1) even though a surfactant free system was used, tip breakup occurred; (2) no clear distinction between tip breakup and total fracture was found for bubbles. Instead the size of the detached tip grew with increasing shear rate. It is of further interest to investigate bubble breakup for higher viscosity ratios ($\lambda = 10^{-6}$–10^{-4}). It is certainly also of interest to go one step further in such fundamental investigations by introducing surfactant into the system. This is expected to either accelerate the tip breakup process dramatically or may directly lead to total bubble fracture.

Acknowledgments The authors would like to thank Rok Gunde for the surface tension measurements, Jan Corsano for building the transparent concentric cylinder device as well as Daniel Kiechl, Bernhard Koller, Peter Bigler, and Bruno Pfister for their technical support.

References

Acrivos A (1983) The breakup of small drops and bubbles in shear flows. Ann NY Acad Sci 404:1

Bentley BJ, Leal LG (1986) An experimental investigation of drop deformation and breakup in steady, two-dimensional linear flows. J Fluid Mech 167:241

Birkhofer BH, Eischen J-C, Megias-Alguacil D, Fischer P, Windhab EJ (2005) Computer-controlled flow cell for the study of particle and drop dynamics in shear flow fields. Ind Eng Chem Res 44:6999

Canedo EL, Favelukis M, Tadmor Z, Talmon Y (1993) An experimental study of bubble deformation in viscous liquids in simple shear flow. AIChE J 39:553

Cerf RJ (1951) Rechercheds theoretiques sur l'effet Maxwell des solutions de macromolecules deformables, 2. Applications de la theorie de la sphere elastique aux solutions de macromolecules en chianes. J Chimie Physique et de physico-chimie biologique 48:85

Chaffey CE, Brenner H (1967) A second-order theory for shear deformation of drops. J Colloid Interface Sci 24:258

Cox RG (1969) The deformation of a drop in a general time-dependent fluid flow. J Fluid Mech 37:601

de Bruijn RA (1993) Tipstreaming of drops in simple shear flows. Chem Eng Sci 48:277

DIN (1976) 53018, Teil 1: Viskosimetrie, Messung der dynamischen Viskositäten and Fliesskurven mit Rotationsvisosimetern mit Standardgeometrie: Normausführung, DIN Deutsches Institut für Normung, Beuth Verlag GmbH, Berlin

Fischer P, Erni P (2007) Emulsion drops in external flow fields—the role of liquid interfaces. Curr Opin Colloid Interface Sci 12:196

Grace HP (1982) Dispersion phenomena in high viscosity immiscible fluid systems and application of static mixers as dispersing devices in such systems. Chem Eng Commun 14:225

Gordillo JM, Perez-Saborid M (2006) Axissymmetric breakup of bubbles at high Reynolds numbers. J Fluid Mech 562:303

Guido S, Greco F (2001) Drop shape under slow steady shear flow and during relaxation, experimental results and comparison with theory. Rheol Acta 40:176

Guido S, Villone M (1998) Three-dimensional shape of a drop under simple shear flow. J Rheol 42:395

Guido S, Greco F, Villone M (1999) Experimental determination of drop shape in slow steady shear flow. J Colloid Interface Sci 219:298

Hinch EJ, Acrivos A (1980) Long slender drops in a simple shear flow. J Fluid Mech 98:305

Karam HJ, Bellinger JC (1968) Deformation and breakup of liquid droplets in a simple shear field. Ind Eng Chem Fundam 4:576

Lasheras JC, Eastwood C, Martínez-Bazán C, Montañés JL (2002) A review of statistical models for the break-up of an immiscible fluid immersed into a fully deverloped turbulent flow. Int J Multiphase Flow 28:247

Maffetone PL, Minale M (1999) Equation of change for ellipsoidal drops in viscous flow. J Non-Newton Fluid Mech 78:227

Müller-Fischer N, Bleuler H, Windhab EJ (2007a) Dynamically enhanced membrane foaming. Chem Eng Sci 62:4409

Müller-Fischer N, Suppiger D, Windhab EJ (2007b) Impact of static pressure and volumetric energy input on the microsctucture of food foam whipped in a rotor-stator device. J Food Eng 80:306

Pozrikidis C (1993) On the transient motion of orderes suspensions of liquid drops. J Fluid Mech 264:301

Rallison JM (1981) A numerical study of the deformation and burst of a viscous drop in general shear flows. J Fluid Mech 109:465

Rallison JM (1984) The deformation of small viscous drops and bubbles in shear flows. Ann Rev Fluid Mech 16:45

Revuelta A, Rodríguez-Rodríguez J, Martínez-Bazán C (2006) Bubble break-up in a straining flow at finite Reynolds numbers. J Fluid Mech 551:175

Risso F, Fabre J (1998) Oscillation and breakup of a bubble immersed in a turbulent flow. J Fluid Mech 372:323

Rodríguez-Rodríguez J, Gordillo JM, Martínez-Bazán C (2006) Breakup time and morphology of drops and bubbles in a high-Reynolds-number flow. J Fluid Mech 548:69

Rust AC, Manga M (2002) Bubble shapes and orientation in low Re simple shear flow. J Colloid Interface Sci 249:476

Stone HA (1994) Dynamics of drop deformation and breakup in viscous fluids. Ann Rev Fluid Mech 26:65

Stone HA, Bentley BJ, Leal LG (1986) An experimental study of transient effects in the breakup of viscous drops. J Fluid Mech 173:131

Taylor GI (1934) The formation of emulsions in definable fields of flow. Proc R Soc Lond Ser A 146:501

Torza S, Cos RG, Mason SG (1972) Particle motions in sheared suspensions: XXVII. Transient and steady deformation and burst of liquid drops. J Colloid Interface Sci 38:395